BBA - Molecular Basis of Disease 1866 (2020) 165843

Contents lists available at ScienceDirect

BBA - Molecular Basis of Disease

journal homepage: www.elsevier.com/locate/bbadis

Copper mediates mitochondrial biogenesis in retinal pigment epithelial cells

M. Aloysius Dhivya[a,b], S. Aberami[a], Sampath Nikhalashree[a,b], J. Biswas[c], Wenjie Liu[d], Joseph Irudayaraj[d], K.N. Sulochana[a], Karunakaran Coral[a,*], S.R. Bharathi Devi[a,*]

[a] R S Mehta Jain Department of Biochemistry and Cell Biology, KBIRVO, Vision Research Foundation, Sankara Nethralaya, College Road, Nungambakkam, Chennai - 6, India
[b] SASTRA deemed to be University, Trichy - Tanjore Road, Thirumalaisamudram, Thanjavur, Tamil Nadu 613401, India
[c] Department of Uveitis, Medical Research Foundation, India
[d] Department of Bioengineering, Cancer Center at Illinois, Micro and Nanotechnology Laboratory, University of Illinois at Urbana-Champaign, Urbana, IL 61801, USA

ARTICLE INFO

Keywords:
Copper
AMD
Mitochondrial biogenesis

ABSTRACT

Age related macular degeneration (AMD) is a multifactorial disease with genetic, biochemical and environmental risk factors. We observed a significant increase in copper levels in choroid-RPE from donor eyeballs with AMD. Adult retinal pigment epithelial cells (ARPE19 cells) exposed to copper in-vitro showed a 2-fold increase in copper influx transporter CTR1 and copper uptake at 50 μM concentration. Further there was 2-fold increase in cytochrome C oxidase activity and a 2-fold increase in the mRNA expression of NRF 2 with copper treatment. There was a significant increase in mitochondrial biogenesis markers PGC1β and TFAM which was confirmed by mitochondrial mass and copy number. On the contrary, in AMD choroid-RPE, the CTR1 mRNA was found to be significantly down-regulated compared to its respective controls. SCO1 and PGC1β mRNA showed an increase in choroid–RPE. Our study proposes copper to play an important role in mitochondrial biogenesis in RPE cells.

1. Introduction

Age related macular degeneration (AMD) is a leading cause of blindness worldwide. The global prevalence of AMD is 196 million in the year 2020 [1]. AMD is a multifactorial disease with genetic, biochemical, nutritional and environmental risk factors [2]. In the early stage of AMD, tiny drusen appear on the retina which are little piles of waste product of the cells. Dry AMD is characterized by pigment discoloration and the presence of drusen. In fact, nearly everyone over 50 years of age has at least one small drusen. Intermediate AMD is characterized by the accumulation of focal or diffuse drusen and hyper- or hypopigmentation of the retinal pigment epithelium (RPE). Advanced AMD can be classified as geographic atrophy (GA; i.e., dry, or non-exudative, AMD), characterized by a sharply delineated area of RPE atrophy and the other choroidal neovascularization (CNV; i.e., wet, or exudative, AMD), which may involve subretinal neovascular membranes; subretinal fluid, exudates, and hemorrhages, pigment epithelial detachment and subretinal/intraretinal scarring. Advanced AMD can result in loss of central visual acuity and lead to severe and permanent visual impairment and blindness. About 10% of all cases of age-related macular degeneration become “Wet” AMD [3,4].

There is evidence that trace elements might play a role in the pathogenesis of AMD. Deposition of metal ions is reported in the order of Ca > Zn > Fe in extracellular deposits of AMD cases [5] Our recent study has shown accumulation of heavy metals like lead, cadmium, chromium, nickel and arsenic in choroid-RPE and retina of donor eyes with AMD [6]. Iron is a potent generator of reactive oxygen species (ROS), whose generation within mitochondria and lysosomes may promote cell death [7]. Iron accumulation has been found in the RPE, Bruch's membrane in early AMD, geographic atrophy, and exudative AMD [8] Iron is suggested as a source of oxidant- . Another study by Biesemeier et al. reported that iron accumulation was seen in melanosomes in donor eyes suffering from AMD compared to age-matched people without AMD [9].

Abbreviations: ARMD, age related macular degeneration; mtDNA, mitochondrial DNA; ARPE-19, adult retinal pigment epithelial 19; HNO_3, concentrated nitric acid; H_2O_2, hydrogen peroxide; GSSG, glutathione disulfide; GAPDH, glyceraldehyde 3-phosphate dehydrogenase; CTR1, copper transporter 1; SCO1, synthesis of cytochrome c oxidase; ERRα, estrogen related receptor α; COX, cytochrome C oxidase; VEGF, vascular endothelial growth factor; ATOX1, antioxidant 1; ATP7A & 7B, copper transporting ATPase 7A & 7B; CCS, copper chaperone for superoxide dismutase; SOD1, superoxide dismutase 1; COX11, cytochrome c oxidase copper chaperone 11; NRF1, nuclear respiratory factor 1; NRF2, nuclear factor erythroid 2-related factor 2; PGC1α & β, peroxisome proliferator-activated receptor gamma coactivator 1-alpha and beta; TFAM, transcription factor A, mitochondrial; MFN2, Mitofusin 2; CO1, cytochrome C oxidase 1; CO2, cytochrome C oxidase 2

* Corresponding authors.
E-mail addresses: drkc@snmail.org (K. Coral), drbarathi@snmail.org (S.R. Bharathi Devi).

https://doi.org/10.1016/j.bbadis.2020.165843
Received 1 October 2019; Received in revised form 29 February 2020; Accepted 19 May 2020
Available online 23 May 2020

Copper and zinc play vital roles in visual cycle and photoreceptor survival [10] and are essential for antioxidant defence mechanisms [11] and for the survival of the retina, which is routinely exposed to high levels of oxidative stress from light and metabolic processes. The aqueous humor trace elements levels in AMD cases show increase in iron and zinc and decrease in copper ions [12]. The tissue levels of copper and zinc are also reported to be decreased in RPE and choroid of AMD cases [13]. A mice model with deficiency of ceruloplasmin a copper carrier and storage protein had been shown to develop retinal iron overload [14]. This shows that copper is essential in maintaining the homeostasis of other elements such as iron and zinc and vice versa.

In this study when we evaluated the elements iron, copper, zinc and calcium in the cadaveric donor choroid-RPE and retinal tissue with AMD changes, surprisingly, copper was found to be significantly increased in choroid–RPE of the late AMD cases whereas iron and zinc showed decrease in both choroid–RPE and retinal tissue. The RPE plays a major role in the inter-cellular tight junctions and restrict the distribution of drugs and other xenobiotics from the choroidal bloodstream into the inner parts of the eye [15]. The RPE also supports visual functions and secretes growth factors, phagocytosis shed photoreceptor outer segments (POS) and provides nutrients to the neural retina [16]. Disturbances in RPE leads to AMD therefore, RPE cells are subjected to intensive medical and pharmaceutical research. ARPE19 cell line is widely used as a cell model to study AMD pathogenesis [17–20]. Copper is an essential trace element, required for the normal cellular functioning and energetics by regulating the level of mitochondrial enzyme cytochrome C oxidase [21]. The pivotal role of this element in regulating mitochondria is unexplored especially in retinal pigment epithelial cells. With tissue level of copper being increased in AMD donor tissue, its effect was investigated in ARPE19 cell model .

2. Materials and methods

2.1. Procurement and assessment of AMD donor eyes

Human Cadaver eyes were obtained from C.U. Shah Eye bank with informed consent obtained from the deceased relative. The age, gender, history of systemic and ocular problems of the donor eyes was recorded. The ophthalmic history of the deceased donors is not available as these donors were not treated in our Institute. All experiments pertaining to this study adhered to the guidelines of the Declaration of Helsinki. Totally 243 eyeballs after removal of cornea were procured from C.U. Shah Eye bank. The eyes were examined by an ophthalmologist cum pathologist by visually seeing the posterior segment of the eye after removal of cornea. Later the globes were grossed and one-half of it was fixed in formalin for 24 h and processed for histopathological examination and the other half of the eyeball was used for elemental analysis.

2.2. Methodology for grossing, sectioning and staining

As described in the earlier report by Aberami et al. [6] where in each eyeball was dissected vertically across the macula to make sure that every single eye is studied for histopathological and elemental analysis. After automated tissue processing was completed, the tissues were embedded with paraffin wax and 5 μm sections were taken. The sections were deparaffinized and then stained using hematoxylin and eosin. Precautions were taken to avoid lipid artifacts due to wax by repeated washing with xylene. The sections stained were evaluated for basal laminar deposits, subretinal hemorrhage, hard, small drusen and thickening and calcification of Bruch's membrane in the macula according to Biswas et al., and were graded as AMD changes and without AMD changes [23]. Further classification as early and late AMD was done based on the Alabama grading system [24].

2.3. Extraction of elements

Samples were collected in trace metal free polypropylene tubes (ABDOS, India). A blank tube containing only 0.2% HNO_3 was processed analogously with the samples. The choroid-RPE and retina, were removed and the wet weight of tissue was recorded. The tissue was homogenized with 1 ml of element free MilliQ water and digested with 1 ml of 30% H_2O_2 in a clean porcelain dish and incubated in hot air oven for 24 h at 75 °C. Further for ashing 0.5 ml of concentrated nitric acid (Fluka, China trace element grade) was added and heated on a Bunsen flame till it dried. The ashed sample was dissolved in 2 ml of 0.2% HNO_3 and centrifuged at 2500 rpm for 10 min. The supernatant was collected and transferred to a sterile polypropylene screw cap tubes (SCT-5 ml) and stored at room temperature.

2.4. Element estimation

The assay of trace elements was done with commercial kit as per manufacturer's protocol (Coral Clinical Systems, India). Copper released from ceruloplasmin in an acidic medium, reacts with (3,5-bromo-2-pyridylazo-N-ethyl-N-(3-sulfopropyl) aniline) Di-Br-PAESA to form a colored complex. Intensity of the complex formed is directly proportional to the amount of copper present in the sample. Iron which is dissociated from transferring-iron complex in weakly acid medium was reduced into the bivalent form by means of ascorbic acid. Ferrous ions give with FerroZine a colored complex: The intensity of the color formed is proportional to the iron concentration. Zinc in alkaline medium reacts with 2-(5-nitro-2-pyridylazo)-5-(N- propyl-N-sulfopropylamino) Nitro-PAPS to form a purple colored complex. Intensity of the complex formed is directly proportional to the amount of zinc present in the sample. Calcium combines specifically with Arsenazo III at a neutral pH to form a blue purple colored complex. Intensity of the color formed is directly proportional to the amount of calcium present in the sample.

2.5. Cell culture

The cell model to study the AMD pathogenesis is adult human retinal pigment epithelial cells (ARPE) 19 (ATCC – CRL 2302) which were cultured using DMEM – F12 (Sigma, USA) medium supplemented with 10% FBS (Gibco, USA) and 0.1× of antimycotic and antibacterial solution (Gibco, USA). The cells were treated with varying concentrations of copper – copper chloride ($CuCl_2$) 50, 100, and 200 μM. Penicillamine at a concentration of 800 μM, was used as copper chelator. The treatment was given in DMEM 5.5 mM glucose supplemented with 1% FBS (Gibco, USA) and antimycotic and antibacterial solution (Gibco, USA).

2.6. Viability assay

MTT (3-(4, 5-dimethythiazolyl-2)-2, 5-diphenyltetrazolium bromide) assay was done to check the effect of $CuCl_2$ at different time points 1, 24, 48 and 72 h on the viability of ARPE19 cells. After treatment with copper the cells were incubated with the MTT reagent and the formazan crystals were dissolved in DMSO and read at 570 nm (Spectramax M2e, Molecular Devices, California).

2.7. Detection of reactive oxygen species (ROS)

The concentration of ROS in ARPE19 cells was detected by measuring the fluorescent signal from the DCFDA (redox-sensitive-fluoroprobe- 2′, 7′-dichlorofluorescein-diacetate). ARPE19 cells exposed to the treatment conditions and with H_2O_2 as a positive control (at a concentration of 100 μM for 1 h) in 96 well plate, were washed in PBS buffer. DCFDA (10 mM) was added in serum-free medium and incubated at 37 °C for 120 min. The fluorescence of DCF in the ARPE19 cells was detected with 525 nm emission wavelength and 485 nm

excitation wavelength in kinetic mode with a 30 min interval.

2.8. Mitochondrial membrane potential assay

The mitochondrial membrane potential was visualized using a fluorescence microscopy using JC-1 dye (Thermofisher) according to the manufacturer's protocol. JC-1 accumulation in mitochondria leads to the aggregate formation emitting red fluorescence while leakage of the dye to the cytoplasm denotes monomer formation giving green fluorescence. ARPE19 cells were seeded in a 96 well plate and treated with copper for 24 h and with H_2O_2 (at a concentration of 100 μM for 1 h as a positive control). Post treatment the cells were washed with PBS and incubated with JC-1 dye at a concentration of 10 ng/ml for 30 min at 37 ˚C. Stained cells were visualized using Zeiss Microscope.

2.9. Estimation of copper in ARPE19 cells

Intracellular copper was measured using atomic absorption spectrophotometer (AAS) Analyst 700 (Perkin Elmer, USA). The cells post exposure to copper at concentrations 15, 50, 100 and 200 μM for 1, 6, 12, 24 and 48 h and penicillamine for 24 h (800 μM) was washed with PBS and lysed using 5:1 nitric acid: perchloric acid (Merck, India) and ashed in a bunsen flame. The ashed samples were dissolved in 1 ml 0.2% nitric acid, centrifuged and the supernatant was used for the estimation of copper. The AAS parameters for the assay are as follows copper hallow cathode lamp at a wavelength of 324.8 nm with the slit length at 0.7 nm was maintained and copper was atomized at 2300 ˚C using a graphite furnace and the absorbance was recorded. The concentration of copper was calculated after calibration with known standards from Perkin Elmer (1 mg/ml concentration).

2.10. RNA extraction and polymerase chain reaction

Total RNA was extracted using TRIzol reagent (Sigma, USA) as per the manufacturer's protocol. It was quantified using nanodrop spectrophotometer. One microgram of the total RNA was converted to cDNA using iScript cDNA synthesis kit (Bio-Rad, USA). Quantitative PCR (qPCR) was done based on SYBR chemistry. qPCR primers were designed using Primer3 software [25]. The list of primers used is given in the table (Table 1). Specificity of the amplified product was based on the melting curve and the fold change was calculated using the $2^{\Delta Ct}_{(\text{treated}-\text{untreated})}$ method. GAPDH was used for normalization [26].

2.11. Immunofluorescence

The cells grown in 4-well chamber slides and exposed to copper treatment for 24 h, were fixed with 4% formaldehyde and permeabilized with 0.1% triton X 100. The cells stained with CTR1 (1:500 Pierce, Thermo Scientific, USA). were captured in ImageXpress Micro Confocal Microscope (Molecular Devices, USA). For staining NRF2, PGC1β and MFN2, the exposed cells were fixed with 4 % formaldehyde and permeabilized with 1 % triton X 100. The cells stained with NRF2 (1:200, Santa Cruz, USA) were captured in Carl Zeiss LSM700 confocal microscopy, while the cells stained with PGC1β (1:200, Santa Cruz, USA) and MFN2 (1:200, Novus Biologicals) were imaged in EVOS FL auto microscope. DAPI was used to stain the nucleus.

2.12. Western blot analysis

ARPE19 cells were lysed using RIPA buffer (50 mM Tris-HCl, 150 mM NaCl, 0.1% Triton X 100, 0.5% sodium deoxycholate, 0.1% SDS and protease inhibitor cocktail (Roche, Switzerland)). The total protein was estimated using BCA kit (Thermo Scientific, USA) and 35–40 μg concentration of protein was used. Twelve percentage resolving gel SDS-PAGE was used, and the blot was transferred to PVDF (GE Healthcare, USA) through semi dry transfer method. Five percent nonfat dry milk in TBST was used as a blocking agent. The blots were incubated overnight with appropriate dilution of primary antibody for CTR1 (1:1000 Pierce, Thermo Scientific, USA), SCO1 (1:500 Santa Cruz Biotechnology, USA), ERRα (1:1000 Cell Signaling Technology), TFAM (1:1000 Cell Signaling Technology) and β-actin (1:1000 Santa Cruz Biotechnology, USA). The overnight incubation was followed by washing and 2 h incubation with the appropriate secondary antibody. The bands on the membrane were detected on exposure with ECL (Bio-Rad, USA) substrate using Flourchem FC3 Gel documentation system. β-Actin was used as a loading control.

Table 1
List of all the primers used in the experiment.

CTR1	FP – 5′ – CTTAGACTGGCTGCCAAAGG – 3′
	RP – 5′ – AGAGTAAGGGGGCCAAAGAA – 3′
SCO1	FP – 5′ – GGGGAGCGTAAAACTGACAA – 3′
	RP – 5′ – TGGGTCAATGCTGATGAAAA – 3′
ATOX1	FP – 5′ – CTGAAGCTGTCTCTCGGGTC – 3′
	RP – 5′ – CAGAGTGTCCATGCTGTGCT – 3′
SOD1	FP – 5′ – GAAGGTGTGGGGAAGCATTA – 3′
	RP – 5′ – ACATTGCCCAAGTCTCCAAC – 3′
CCS	FP – 5′ – ACACACCACTCTACCCAGCC – 3′
	RP – 5′ – CAGGGGTCAGCTGTAGGAAG – 3′
COX11	FP – 5′ – CAGAAATATATGTGGTGCCAG – 3′
	RP – 5′ – ATACTGTCCAGCTTCAAATG – 3′
ATP7A	FP – 5′ – GAATGAGCCGTTGGTAGTAATAGC – 3′
	RP – 5′ – TCCTTCCTCCTTGTCTTGAACTG – 3′
ATP7B	FP – 5′ – ACCCGGAAGCACTGTAATTG – 3′
	RP – 5′ – TCTGAGCCTCTTCCACCAGT – 3′
GAPDH	FP – 5′ – AGATCATCAGCAATGCCT – 3′
	RP – 5′ – TGGTCATGAGCTCTTCCA – 3′
NRF2	FP – 5′ – GTGTGGCATCACCAGAACAC – 3′
	RP – 5′ – TTCCAGGGGCACTATCTAGC – 3′
NRF1	FP – 5′ – TACTCGTGTGGGACAGCAAG – 3′
	RP – 5′ – GCACCACATTCTCCAAAGGT – 3′
PGC1α	FP – 5′ – CCTTGCAGCACAAGAAAACA – 3′
	RP – 5′ – CTGCTTCGTCGTCAAAAACA – 3′
PGC1β	FP – 5′ – AACTATCTCGCTGACACGCA – 3′
	RP – 5′ – GAGTTCTCTGGGCACCACTG – 3′
TFAM	FP – 5′ – TCTGTCTGACTCTGAAAAGG – 3′
	RP – 5′ – CTACTTTTAACACTCCTCAGC – 3′
ERRα	FP – 5′ – CACAAGGAAGAGGAGGATGG – 3′
	RP – 5′ – CACAGGATGCCACACCATAG – 3′
VEGF	FP – 5′ – GTCCAACTTCTGGGCTGTTCTC – 3′
	RP – 5′ – CCCCTCTCCTCTTCCTTCTCTT – 3′

2.13. Mitochondrial copy number

Total DNA from the ARPE19 cells was isolated using DNeasy Blood and Tissue kit (Qiagen, Germany) based on the manufacturer's protocol. The isolated DNA was quantified using Nanodrop Spectrometer and 3 μg was used for the quantitative PCR reaction. The table (Table 2) gives primers used for the qPCR reaction. The calculation of fold change for determining the mitochondrial DNA content was based on the protocol as described by Rooney et al. [27].

Table 2
Primers used for the analysis of mitochondrial copy number.

MTCO1	FP – 5′ – ATACCAAACGCCCCTCTTCG – 3′
	RP – 5′ – TGTTGAGGTTGCGGTCTGTT – 3′
MTCO2	FP – 5′ – GTACTCCCGATTGAAGCCCC – 3′
	RP – 5′ – ACCGTAGTATACCCCCGGTC – 3′
MTCO3	FP – 5′ – GATTTCACTTCCACTCCATAACG – 3′
	RP – 5′ – CTTCTAGGGGATTTAGCGGG – 3′
SDHA	FP – 5′ – CAAGGCGAAAGGTTTATGGA – 3′
	RP – 5′ – AGCGAAGATCATGGCTGTCT – 3′

2.14. Enzymatic activities of cytochrome c oxidase (COX) and citrate synthase (CS)

COX a large multi-subunit enzyme in the inner membrane of the mitochondria, plays a vital role in aerobic respiration, activity of this enzyme on ARPE19 cell lysate was measured based on a modified protocol of Spinazzi, M. et., al. [28]. Briefly, 139 μl of distilled water was added in a 96 well microtiter plate with 50 μl potassium phosphate buffer (100 mM, pH 7), 10 μl reduced ferrocytochrome *c* (1 mM reduced by 1 M DTT) and the baseline activity was read at 550 nm for 2 min. Sample volume of 1 μl was added (2 μg of cell lysate), mixed and the decrease in absorbance at 550 nm for 3 min was monitored. COX activity was determined by measuring the decrease in absorbance caused by oxidation of ferrocytochrome *c* to ferricytochrome *c*. CS activity was measured in the presence of acetyl-CoA and oxaloacetate by monitoring the release of CoASH coupled to 5′5-dithiobis (2-nitrobenzoic) acid at 412 nm [29]. COX activity was expressed as a ratio normalized to that of CS activity.

2.15. Transient expression of CTR1-mCherry and SCO1-EGFP in ARPE19 cells

Around 8000 ARPE19 cells were plated on an 18 mm round No.1 coverslip (precoated with poly-D-lysine) in a 12 well plate and grown unto 70% confluency. Then starved overnight with DMEM/F12 + 1% FBS. The cells were transiently transfected with SCO1-EGFP and CTR1-mCherry with Lipofectamine 2000 according to the manufacture's instruction.

2.16. Fluorescence lifetime imaging based Förster Resonance Energy Transfer for CTR1-SCO1 interaction

Fluorescence lifetime imaging (FLIM) was performed with an Alba (ISS, Champaign, USA) confocal scanning time-resolved imaging system. Details of the instrumentation are as described previously [30,31]. A 488 nm picosecond pulsed laser at 50 MHz repetition rate was used to excite EGFP through an apochromatic water immersion objective (60×, NA = 1.2, Olympus). Photons were then collected by the same objective, reflected by a 560 dichroic filter (Chroma), and passed through a 50 μm pinhole and a band-pass filter (520/53, Chroma) before reaching an avalanche photodiode (SPCM-AQRH-15, Excelitas). Detected photons were stored in Time-tagged time-resolved format and generate a Time-correlated single photon counting (TCSPC) histogram (Becker and Hickl). The laser power was controlled to have a peak photon value of ~105 in the TCSPC histogram. Fluorescence lifetime (τ) was obtained by fitting the TCSPC decay pattern as $F(t) = F_0 e^{-t/\tau}$ (1). Förster Resonance Energy Transfer (FRET) was implemented to assess the potential molecular interaction between SCO1-EGFP and CTR1-mCherry. The FRET efficiency was estimated based on the following equation: $E = 1 - {}^{\tau_{da}}/_{\tau_d}$, (2) where τ_{da} is the lifetime of dual transient transfected SCO1-EGFP/CTR1-mCherry cells, and τ_d is the lifetime of transient transfected SCO1-EGFP cells. FRET E larger than 5% is deemed significant.

2.17. ELISA for VEGF protein

The secretary VEGF protein levels in the conditioned media were quantified using VEGF TMB ELISA kit (Peprotech, USA) as per the manufacturer's protocol.

2.18. MitoTracker Red

The cells were grown in chamber slides and exposed to the above-mentioned conditions. After 24 h, the media was removed and pre-warmed (37 °C) medium with MitoTracker Red CMXRos (Invitrogen, USA) was added at the optimized concentration. The cells were incubated for 30 min under growth conditions following which the medium was removed and fresh buffer was added. The cells were viewed, and the pictures were captured in EVOS FL Auto microscope (Thermo Fisher, USA) and the intensity was calculated using the manufacturer software. The higher magnification images of the mitochondria with MitoTracker Red staining were studied using Carl Zeiss LSM700 confocal microscopy.

2.19. mRNA expression in tissue samples

RNA from the choroid-RPE tissues were isolated based on the manufacturer's protocol using Qiagen RNA isolation kit (Qiagen, Netherlands). The transcript levels of genes, CTR1 (influx chaperone), ATP7A and ATP7B (efflux chaperone), SCO1 (mitochondrial chaperone), PGC1α and β and ERRα (mitochondrial biogenesis markers) and VEGF were quantified. Total number of choroid RPE tissues used for expression study was 32 out of which 13 were control and 11 early AMD and 8 late AMD.

2.20. Statistical analysis

All statistical analysis was done using Graph Prism 7.01. Results are expressed as means ± standard deviations, standard error mean. The Mann-Whitney test was performed for comparison of tissue sample and for in vitro experiments one-way ANOVA, posthoc Dunnett's test was used. All experiments were repeated at least three times for standard deviation calculations. The copper treatment was compared to their controls and penicillamine treatments were compared to their respected copper treated condition for statistical analysis. A p value < 0.05 was considered statistically significant.

3. Results

The demographic details of the donor eyeballs collected for the study were tabulated (Table 3). The AMD changes were assessed after histopathological evaluation. The sections were stained and observed for basal laminar deposits, subretinal hemorrhage, drusen and thickening of Bruch's membrane and was graded based on modified Sarks classification [23]. AMD changes as assessed by a pathologist are listed in Table 4. The number of donor eyes with AMD changes was found to be 55 in which 39 were graded as early AMD and 16 were graded as late AMD and those with no AMD changes were 188 which are referred to as controls in this study. The power analysis was 0.8 as assessed by G*power. Earlier case control studies in AMD have used a ratio of 1:3 [32–34] similar to our study.

Table 3
Demographic details of the donor eyes.

Particulars	No. of subjects
Number of patients	243
Age - Male and female (years)	81 ± 8.0, 80 ± 9.0
Male:female	122:121
General medical history	
Cardio respiratory arrest	137
Pulmonary edema	03
Tuberculosis	02
Natural death	73
Lung cancer	02
Encephalopathy	03
Carcinoma	02
Renal failure	05
Cardiac pulmonary	06
Cerebral hemorrhage	02
Seizures	02
Nephrotic syndrome	02
Respiratory failure	04

Table 4
Histopathological finding of the donor eyes.

S. no	ARMD changes in eyeballs	No of eyeballs
1.	Drusen (hard and soft)	41
2.	RPE atrophy	7
3.	Basal laminal deposits (BLD)	1
4.	RPE and photoreceptor degeneration	4
5.	Sub retinal hemorrhage	1
6.	Sub retinal scar	1

3.1. Quantitative detection of trace elements

The tissues were subjected to elemental extraction and the trace elements like Cu, Zn, Fe, Ca was quantified (Table 5) with the respective control samples. The AMD cases were grouped as early and late based on the Alabama classification. Cu levels were mildly increased in the early AMD choroid RPE tissues (15.42 ± 2.2 vs 14.65 ± 0.99) and it was significantly increased in late AMD choroid RPE tissues when compared to control (24.04 ± 4.87 vs 14.65 ± 0.99). In case of retina the copper levels were significantly decreased in early AMD retinal tissue (13.07 ± 1.34 vs 22.09 ± 1.66) with a mild increase in the copper levels in late AMD retina tissues when compared to its control (25.16 ± 5.11 vs 22.09 ± 1.66). The levels of Zn were significantly decreased in both early and late AMD in choroid RPE when compared to its controls, whereas it is decreased significantly in late AMD retina when compared to control. Iron was significantly decreased in both choroid and retina of late AMD. Calcium was significantly decreased in early AMD choroid RPE and showed no change in late AMD. There was no change in calcium levels in both early and late AMD retina tissues when compared to their controls. The increase in copper levels and decrease in zinc and Iron in the choroid RPE of the AMD donor eyes was intriguing us to further explore the role of copper in regulating mitochondrial biogenesis using ARPE19 cells as a model.

3.2. Viability and intracellular copper levels

Copper concentration range from 6 to 7 μg/g tissue in choroid RPE and 9 to 14 μg/g tissue in retina of normal donor eyes which is equivalent to 95 μM in choroid RPE and 142 μM in retina [13]. So, based on the tissue copper levels reported earlier and observed by us we have selected the range of copper to be tested in vitro in ARPE19 cells from 50 to 200 μM. The effect of copper on the viability of ARPE19 cells was done by MTT assay (50–200 μM) for varying time points of 1, 24, 48 and 72 h. There was no cytotoxicity until 24 h of Cu tested but cell death was seen at 72 h at all concentrations of copper (Fig. 1A). Secondly, to evaluate the copper entry into the cells, the intracellular copper concentration was validated using AAS analysis. Maximum copper uptake was seen at 24 h at all concentrations of copper (Fig. 1B). There was a decrease in the copper uptake with penicillamine + Cu co-treatment (Fig. 1C). Further the protein levels of the copper transporter CTR1 showed a significant increase at 24 h at all concentrations of copper tested and the penicillamine + Cu co-treatment decreased CTR1 protein levels. The same was evident in immunofluorescence (Fig. 1D & F). The mRNA expression of the efflux chaperones ATP7A and B were unaltered at all concentrations of Cu at 24 h (Fig. 1E). These results prove entry of copper into the cell at the tested concentrations.

3.3. Intracellular copper chaperones

Copper is required for mitochondrial cytochrome C oxidase activity and for the antioxidant defence protein Superoxide dismutase. The copper chaperones cytochrome C oxidase assembly protein (SCO1) and cytochrome C oxidase copper chaperone (COX11) carries the copper and deliver it to the mitochondria. Chaperone for Superoxide Dismutase (CCS) transport copper to the superoxide dismutase 1 enzyme (SOD1). Hence, we assessed these intracellular copper chaperones in ARPE19 cells after copper treatment. The mRNA levels of CCS were unaltered in all the concentrations of copper but showed a significant increase only with penicillamine co treatment while it was decreased with penicillamine alone. Similar to CCS, SOD1 mRNA expression was unaltered with copper treatment but surprisingly with penicillamine alone it was increased. SCO1 was significantly increased from 50 to 200 μM Cu indicating delivery of copper to mitochondria. But penicillamine alone and penicillamine + Cu co-treatment did not bring down SCO1 mRNA expression (Fig. 2A). At the level of proteins SCO1 showed a dose dependent increase at all concentration of copper treatment and as well as in penicillamine + Cu co-treatment (Fig. 2B). SCO1 has been reported to play a role in oxidative defence [35]. We speculated the increase in SCO1 is mediated by ROS production. It is also known that SCO1 is reported to be essential for maintaining and sustaining the expression of CTR1 at the plasma membrane [36] which was observed in our results. The other mitochondrial chaperone COX11 mRNA levels did not show change with copper treatment as well as penicillamine + Cu co-treatment but penicillamine alone decreased its expression significantly (Fig. 2A). The effect of penicillamine shows that complete copper chelation decreases mitochondrial chaperone expression. This intrigued us to further investigate the SCO1 protein, so we transiently transfected

Table 5
Concentration of trace elements in ARMD and controls.

Element	Control Concentration (μg/g wet weight) Mean ± SEM (N) Range	Early AMD Concentration (μg/g wet weight) Mean ± SEM (N) Range	Late AMD Concentration (μg/g wet weight) Mean ± SEM (N) Range	*p* value Ctrl vs early AMD = #; Ctrl vs late AMD = †; Early vs late AMD = $
Copper Ch RPE	14.65 ± 0.99 (N = 149) 0.67–52.65	15.42 ± 2.20 (N = 35) 3.02–56.15	24.04 ± 4.87 (N = 14) 6.78–59.7	# = 0.6709; † = 0.0413*; $ = 0.1632;
Copper retina	22.09 ± 1.66 (N = 153) 0.19–95.8	13.07 ± 1.34 (N = 36) 0.86–34.06	25.16 ± 5.11 (N = 15) 3.31–69.56	# = 0.0459*; † = 0.3871; $ = 0.0461*;
Zinc Ch RPE	53.69 ± 2.61 (N = 154) 5.58–145.17	40.15 ± 3.92 (N = 36) 6.85–111.94	30.79 ± 6.42 (N = 15) 6.8–78.57	# = 0.0357*; † = 0.0052**; $ = 0.1394;
Zinc retina	69.37 ± 3.60 (N = 148) 9.13–224.72	64.12 ± 6.75 (N = 37) 11.6–161.28	53.30 ± 12.82 (N = 15) 7.68–156.95	# = 0.6456; † = 0.0486*; $ = 0.1825;
Iron Ch RPE	47.66 ± 2.63 (N = 154) 3.77–177.69	48.55 ± 4.76 (N = 39) 8.84–118.87	26.35 ± 4.80 (N = 15) 6.14–59.43	# = 0.7507; † = 0.0057**; $ = 0.0058**;
Iron retina	48.52 ± 3.23 (N = 145) 8.57–218.45	39.50 ± 5.35 (N = 38) 4.25–155.1	25.16 ± 5.11 (N = 15) 3.31–69.56	# = 0.1350; † = 0.0449*; $ = 0.4318;
Calcium Ch RPE	1.56 ± 0.17 (N = 154) 0.05–18.18	0.96 ± 0.15 (N = 37) 0.0–3.37	1.60 ± 0.27 (N = 16) 0.02–3.69	# = 0.0122*; † = 0.2846; $ = 0.0234*;
Calcium retina	3.13 ± 0.25 (N = 153) 0.0–14.46	2.57 ± 0.33 (N = 39) 0.0–7.99	3.08 ± 0.67 (N = 15) 0.35–8.84	# = 0.7152; † = 0.7135; $ = 0.7064;

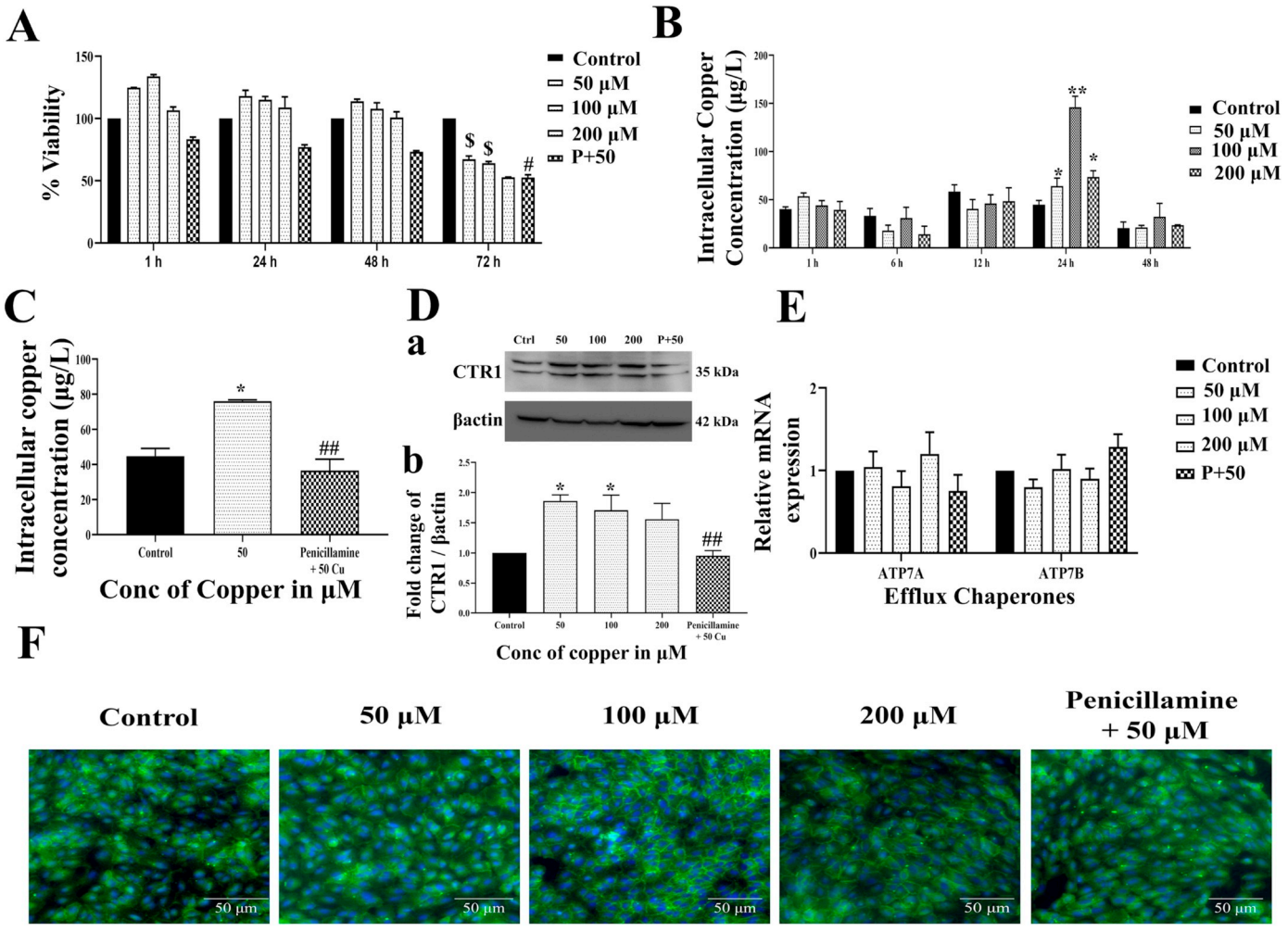

Fig. 1. Viability and expression of intracellular and extracellular chaperone on copper treatment to ARPE19 cells. (A) MTT assay to test the viability of ARPE19 cells on copper exposure. (B) Copper uptake was done using AAS at varying concentrations and time points (C) Copper uptake for penicillamine + Cu co-treatment (P + 50). (D (a)) Western blot for CTR1 protein at 24 h (b) densitogram for CTR1 western blot done using Alpha view software. (E) The mRNA expression levels of the efflux chaperones ATP7A and ATP7B on copper exposure. (F) Localization of CTR1 at varying concentration of copper and with penicillamine + Cu co-treatment (P + 50). $^{*}p \leq 0.05$; $^{**}p \leq 0.01$; $^{\$}p \leq 0.05$ when compared to control. $^{\#}p \leq 0.05$; $^{\#\#}p \leq 0.01$ when compared to 50 µM Copper treatment.

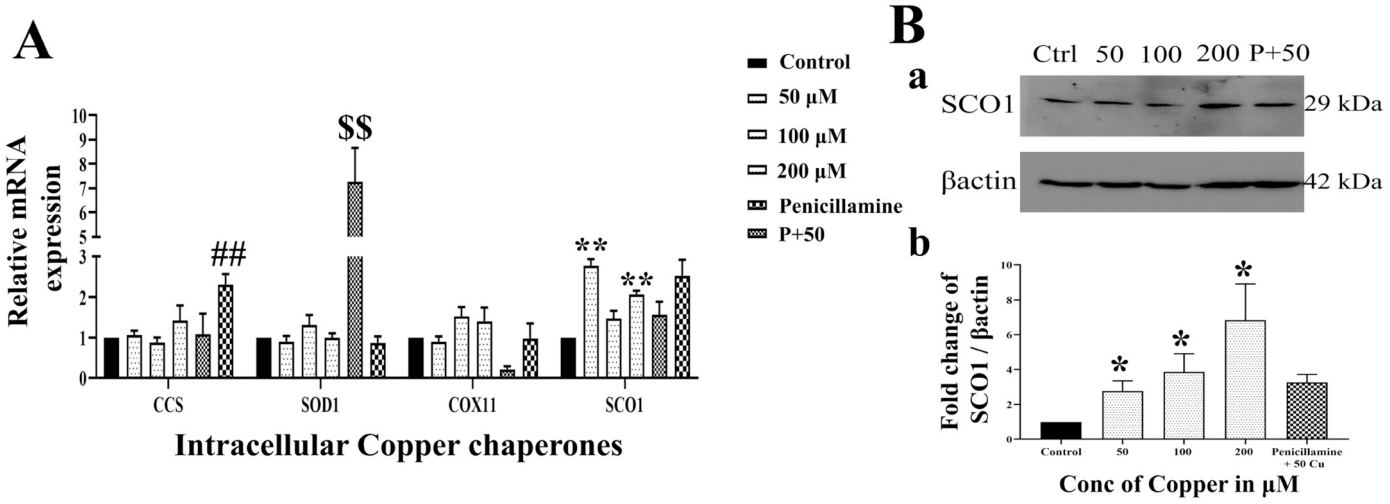

Fig. 2. Expression levels of intracellular copper Chaperones. (A) mRNA expression levels of copper chaperones CCS, SOD1, SCO1 and COX11 at 24 h was assessed by qPCR using GAPDH as internal control. (B) (a) Protein levels of SCO1 was done using western blotting at 24 h. (b) the densitogram for SCO1 western blot was plotted using Alpha view software. $^{*}p \leq 0.05$; $^{**}p \leq 0.01$; $^{\$\$}p \leq 0.01$ when compared to control. $^{\#\#}p \leq 0.01$ when compared to copper 50 µM.

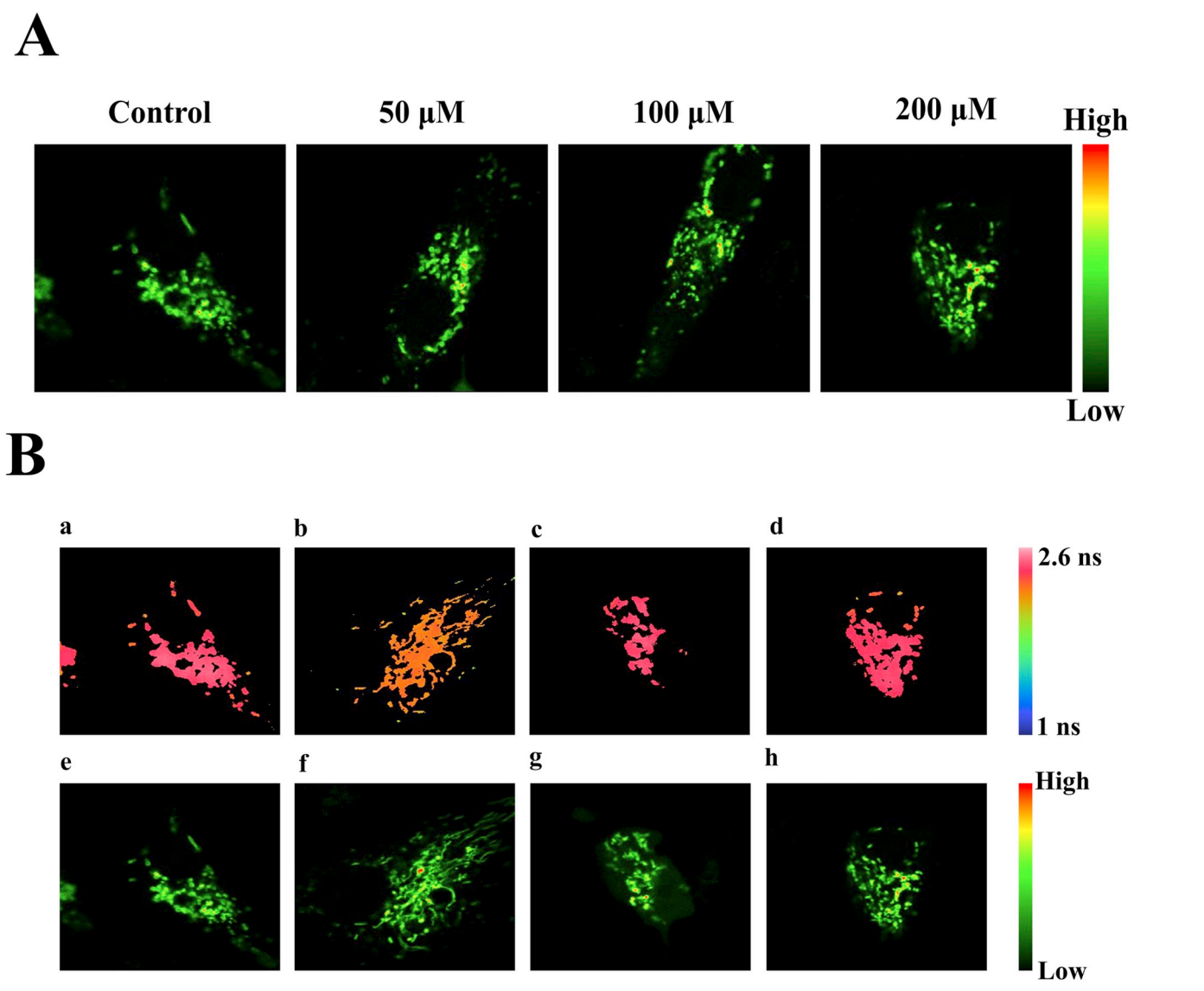

(caption on next page)

Fig. 3. SCO1 expression variation with copper treatment.
(A) Confocal images of SCO1-EGFP under different copper exposure at 24 h in ARPE19 cells. B: Typical fluorescence lifetime image of cells with (a) SCO1-EGFP without copper exposure. (b) Co-expression of CTR1-mCherry and SCO1-EGFP with reduced fluorescence lifetime without copper exposure. (c) Co-expression of CTR1-mCherry and SCO1-EGFP with copper exposure. (d) SCO1-EGFP with 200 μM copper exposure shows no change in fluorescence lifetime. (e–f) Corresponding confocal images without lifetime information in (a–d). Scale bar = 5 μM. (C) FLIM-FRET analysis of SCO1-EGFP and CTR1-mCherry. (a) Fluorescence lifetime of SCO1-EGFP under different copper exposure shows no significant decrease in fluorescence lifetime. (b) Fluorescence lifetime of co-expression cells with SCO1-EGFP and CTR1-mCherry under various copper exposure conditions. (c) Calculated FRET efficiency (FRET E, in %) of SCO1-EGFP and CTR1-mCherry under various copper exposure. (d) Typical TCSPC graph of single cell lifetime with SCO1-EGFP (donor only) and SCO1-EGFP/CTR1-mCherry (FRET). N ~ 15 cells from at least three independent experiments.

SCO1- EGFP in ARPE19 cells and treated with varying concentrations of copper. The SCO1-EGFP intensity pattern was increased with copper treatment and showed perinuclear and cytoplasmic localization pattern (Fig. 3A). This corresponds well with our observation of increased CTR1 protein expression in the cell membrane (Fig. 1F). Further we transfected SCO1-EGFP and CTR1-mCherry together in RPE cells to understand their association on copper treatment by FLIM-FRET analysis. We found that there is a subpopulation of cells with FRET efficiency > 5%, indicating a potential interaction between SCO1-EGFP and CTR1-mCherry in the absence of copper. Once copper was added, FRET efficiency between SCO1-EGFP and CTR1-mCherry dropped to non-significant level, indicating loss of interaction between these proteins (Fig. 3B and C).

3.4. Effect of copper uptake on cellular ROS and mitochondrial membrane potential

Copper is an important player in ROS production through Fenton's reaction and ROS generation modulates mitochondrial membrane potential. There was increased ROS production seen in DCFDA assay in copper treatment as well as in penicillamine + Cu co-treatment (Fig. 4A). Although, ROS production was similar in both copper treated and penicillamine + Cu co-treatment, the JC-1 staining showed enhanced monomer formation indicating decreased mitochondrial membrane potential when copper was chelated. Interestingly, JC-1 staining showed increased JC aggregates in copper treatment illustrating the role of copper in maintaining the mitochondrial membrane potential

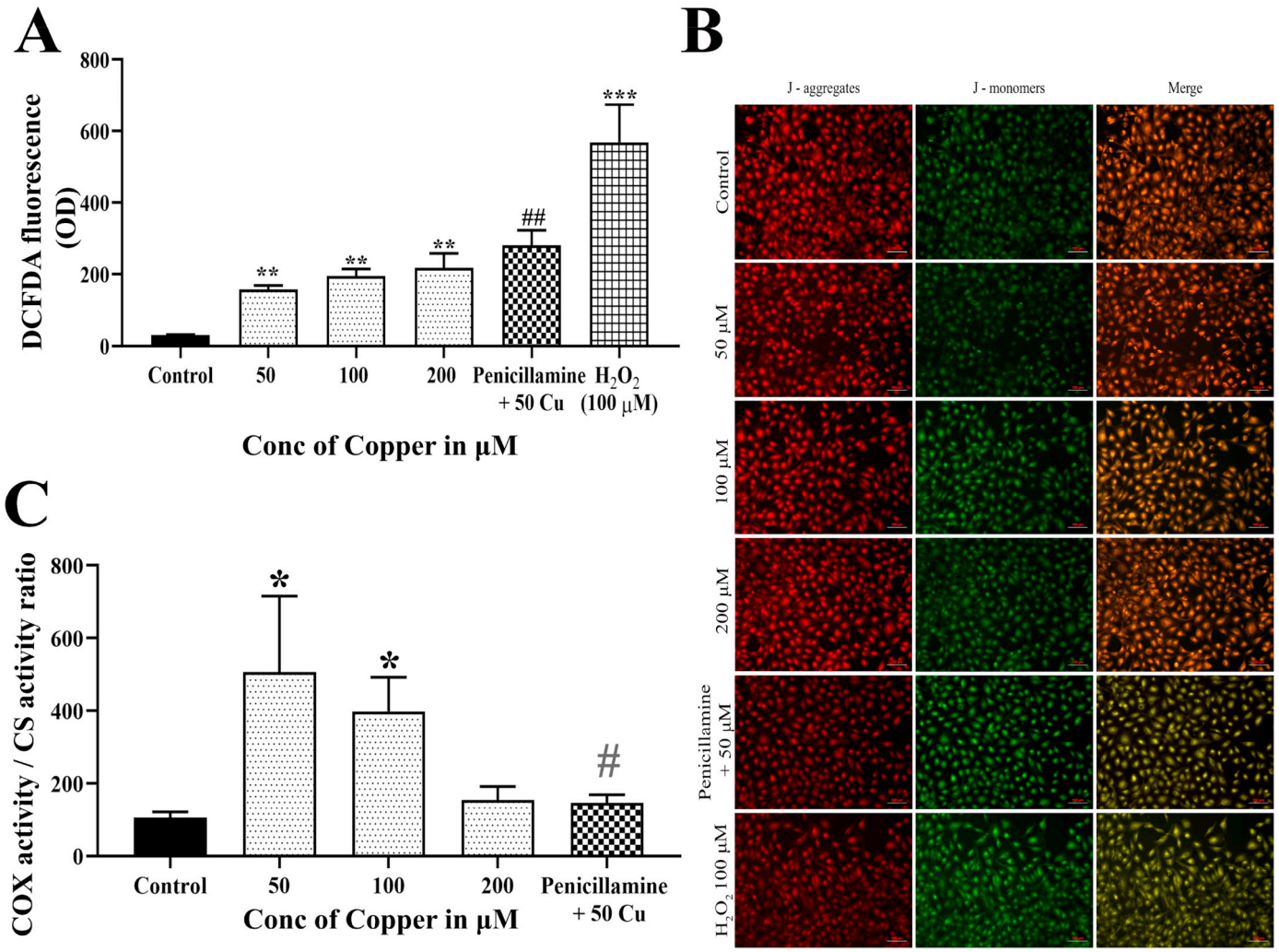

Fig. 4. Effect of copper uptake on cellular ROS and mitochondrial membrane potential (A) ROS was measured using DCFDA assay with positive H_2O_2 (100 μM) control at 24 h treatment with copper. (B) Mitochondrial membrane potential was measured using JC-1 dye. (C) The ratio between cytochrome c oxidase and citrate synthase activity at varying concentration of copper and with penicillamine + Cu co-treatment (P + 50). *$p \leq 0.05$; **$p \leq 0.01$; ***$p \leq 0.001$ when compared to control. $^{\#}p \leq 0.05$; $^{\#\#}p \leq 0.01$ when compared to copper 50 μM treatment.

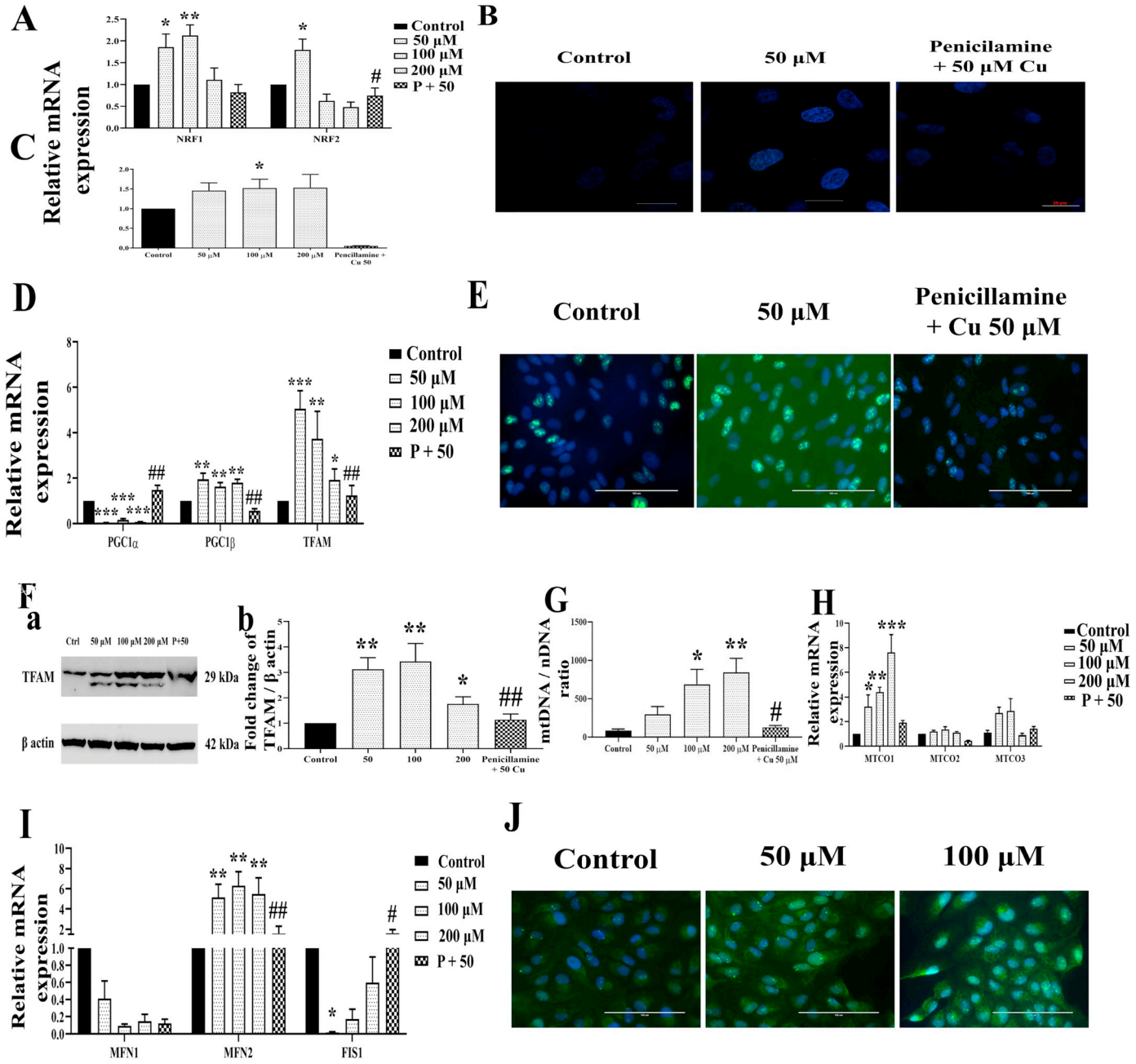

Fig. 5. Expression of mitochondrial biogenesis markers in ARPE19 cells. (A) The mRNA expression of NRF1 and NRF2 with varying concentrations of copper and with penicillamine + Cu co-treatment (P + 50) at 24 h. (B) Nuclear localization of NRF2 on copper treatment at 24 h. (C) mRNA expression of Heme oxygenase, a downstream target of NRF2. (D) mRNA expression of mitochondrial transcription factors TFAM, PGC1α and β on copper treatment at 24 h. (E) immunofluorescence imaging of PGC1β in 50 μM concentration of copper and with penicillamine + Cu co-treatment (P + 50). (F) (a) Western blotting for TFAM protein at 24 h with varying concentrations of copper. (b) Densitogram of TFAM western blot using Alpha view software. (G) Ratio between mitochondrial DNA (COX1) and nuclear DNA (SDHA) (H) mRNA expression of COX enzyme subunits at varying concentrations of copper at 24 h. (I) mRNA expression levels of Mitofusin protein 1 and 2 and Fission 1 in copper and with penicillamine + Cu co-treatment (P + 50). (J) Immunofluorescence imaging of Mitofusin 2 at varying concentration of copper at 24 h. $^{*}p \leq 0.05$; $^{**}p \leq 0.01$; $^{***}p \leq 0.001$ when compared to control. $^{\#}p \leq 0.05$; $^{\#\#}p \leq 0.01$ when compared to copper 50 μM treatment.

(Fig. 4B). Since copper is an important cofactor in the cytochrome C oxidase complex. We tested the activity of cytochrome C oxidase on copper treatment and it showed a significant increase at 50 and 100 μM copper concentration and decreased with penicillamine + Cu co-treatment when normalized to citrate synthase activity (Fig. 4C). This increased activity of cytochrome C oxidase intrigued us to apprehend the role of copper in mitochondria.

3.5. Role of copper in mitochondrial biogenesis

NRF2 is a basic leucine zipper (bZIP) protein that controls the basal and induced expression of an array of antioxidant response element-dependent genes to regulate the physiological and pathophysiological outcomes of oxidative stress. NRF2 is ubiquitously and constitutively expressed by all cells. The NRF2 gene promoter presents several

regulatory sequences which include xenobiotic response element, ARE-like sequences which allows its autoregulation, TRE site that is activated by the oncogenes, NF-κB binding site that responds to inflammatory stimuli [37,38]. NRF1 and NRF2 transcription factors are also modulated by copper [39]. We observed a significant increase in NRF1 and 2 at 50 μM Cu (Fig. 5A) and also its translocation to nucleus on copper treatment (Fig. 5B) and its downstream target gene HO-1 (heme oxygenase) (Fig. 5C).

NRF 1 & 2 can regulate mitochondrial transcription factors like peroxisome proliferator-activated receptor gamma coactivator1 (PGC1) α and β [40]. PGC 1α and β are the main regulators of mitochondrial activity and biogenesis [41]. Therefore, the mitochondrial biogenesis transcription factors were analyzed with copper treatment. We found that there was a significant increase in PGC1β and TFAM mRNA expression with copper treatment from 50 to 200 μM. Surprisingly, the other transcription factor PGC1α was found to be significantly down regulated in all concentrations of copper. PGC1β protein expression was also increased on treatment with copper at 50 μM and decreased with penicillamine + Cu co treatment (Fig. 5D and E). The biogenesis marker TFAM protein was found be significantly increased from 50 to 200 μM Cu and decreased with penicillamine + Cu co-treatment (Fig. 5F). To further establish that there is true mitochondrial biogenesis, mitochondrial copy number was quantified by using a qPCR-based method. Initially the mRNA expression of cytochrome C oxidase coding genes mtCOI, mtCOII, mtCOIII were analyzed and we found a significant increase in the expression of mtCO1 at all concentrations of copper (Fig. 5G). It was also found that there was a dose dependent increase in COX1/SDHA ratio with copper treatment. Whereas penicillamine + Cu co-treatment showed significantly decreased COX1/SDHA ratio when compared to copper treated (Fig. 5H).

Further the downstream target of PGC1β, Mitofusin 2 (MFN2) an outer mitochondrial membrane fusion protein, which activates mitochondrial metabolism also showed a significant increase at the level of mRNA and protein with copper treatment. While in penicillamine + co-treatment MFN2 transcript was significantly decreased. Interestingly the Fission 1 (FIS1) protein involved in the fragmentation of the mitochondrial network expression, was decreased at 50 μM copper treatment (Fig. 5I & J). The inverse relationship of MFN2 and FIS1 has to be further studied. MitoTracker staining of mitochondria also showed a significant increase in intensity with copper treatment and decreased intensity in penicillamine + Cu co-treatment (Fig. 6). These results show that there is mitochondrial biogenesis with copper treatment.

3.6. Effect of copper on augmenting cellular survival by enhancing ERRα and VEGF

The other downstream target of PGC1β, is estrogen related receptor alpha (ERRα) a nuclear receptor and an inducer of VEGF [42,43]. The mRNA and protein expression of ERRα was found to be significantly increased in all concentrations of copper similar to PGC1β (Fig. 7A & B). The levels of ERRα decreased in the penicillamine + Cu co-treatment when compared to copper treatment. VEGF showed an increase at all concentrations of copper compared to control in both mRNA and protein. Penicillamine + Cu co-treatment showed decreased expression levels of VEGF compared to copper treated (Fig. 7C & D). ERRα has also been reported as an inducer of MFN2 [44] and in our study we observed a simultaneous increase of both ERRα and MFN2 in copper treatment.

3.7. Assessment of copper related chaperones in the AMD tissue samples

To further explore these molecules at the level of tissues, the gene expression of the copper influx, efflux and related copper chaperones was performed in the choroid-RPE tissue of the AMD cases as this a composite of both RPE and choroidal cells. The mRNA expression of the influx chaperone CTR1 was found to be significantly down regulated in early AMD, when compared to its respective controls unlike the increased protein expression seen in ARPE19 copper treated cells. DMT1 (a divalent metal transporter) showed an increase in early and late choroid RPE tissue. Whereas the expression of the mitochondrial chaperone SCO1 was increased in AMD choroid RPE tissue similar to the cell culture data. The PGC1α was decreased significantly in early and late AMD cases but PGC1β was significantly down regulated in early AMD and mildly increased in late AMD cases similar to the cell culture data inference. ERRα was decreased significantly in early and late AMD cases whereas VEGF showed increase in early choroid RPE but was decreased in late AMD. The efflux chaperone ATP7A and ATP7B was significantly increased in early AMD of choroid RPE (Fig. 8). These

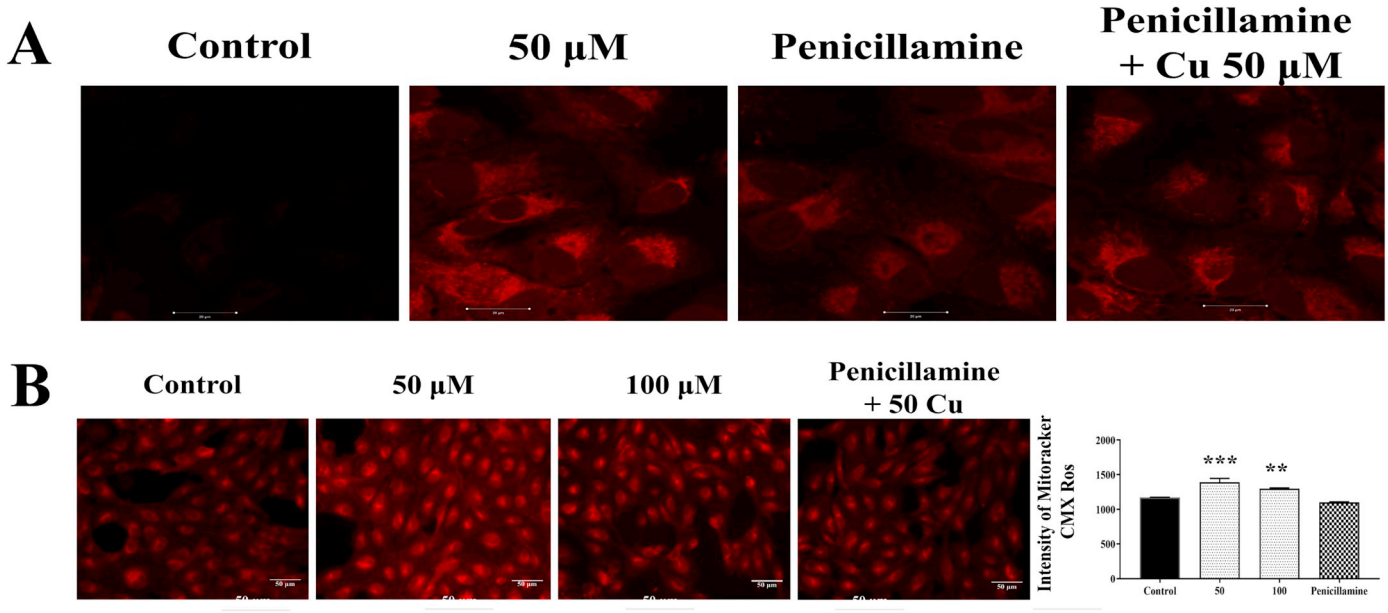

Fig. 6. Mitochondrial Mass. (A) Mitochondria was stained using MitoTracker CMX Ros and pictured at higher magnification (60×) using Carl Zeiss LSM700 confocal microscopy. (B) The stained mitochondrial pictures were captured at a lower magnification (20×) and the intensity of the stain was analyzed using Image J software. $^{**}p \leq 0.01$; $^{***}p \leq 0.001$ when compared to control.

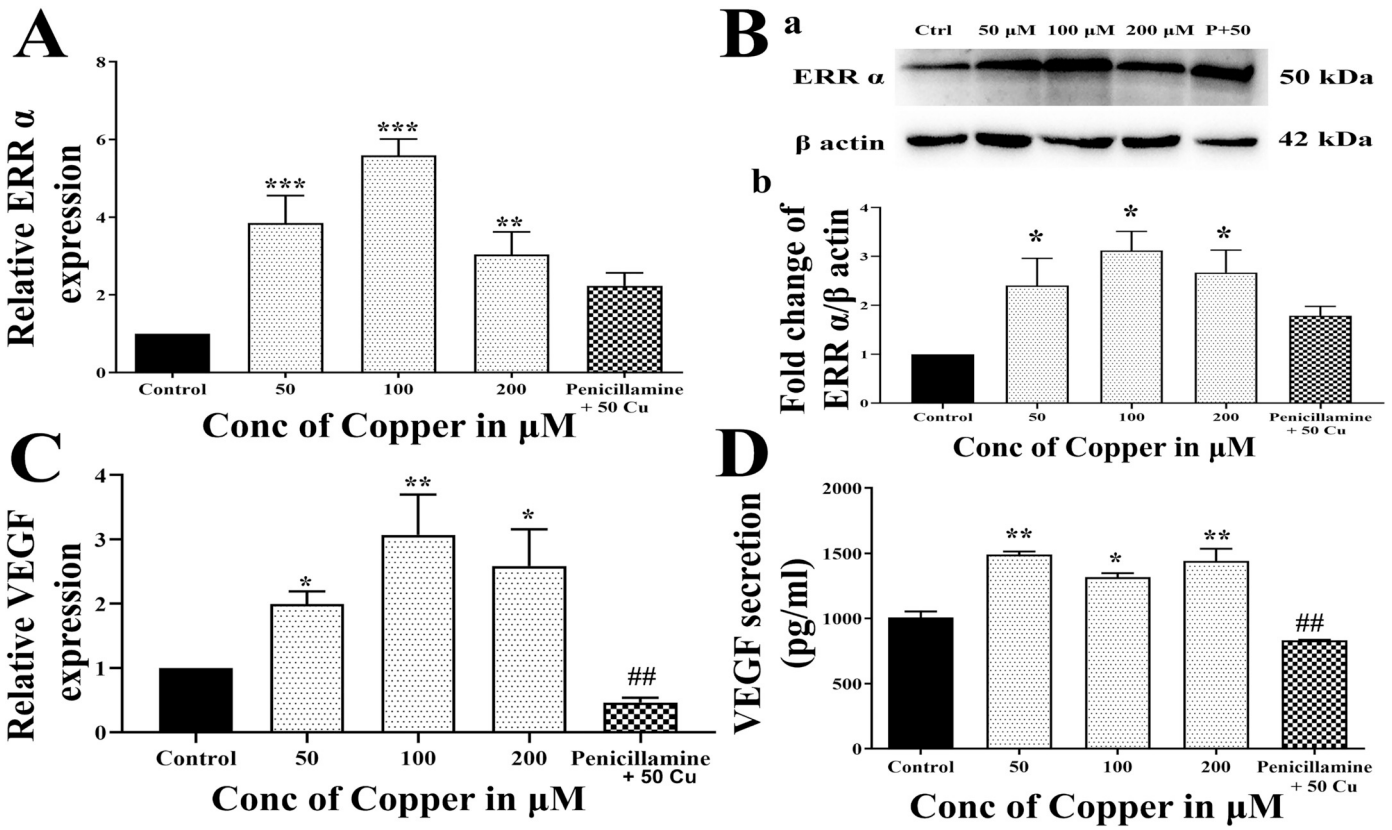

Fig. 7. Expression levels of ERRα and VEGF. (A) mRNA expression levels of Estrogen Related Receptor α (ERRα) at varying copper concentration and with penicillamine + Cu co-treatment (P + 50) at 24 h. (B) Protein levels of ERRα by western blot at 24 h (C) mRNA expression levels of vascular endothelial growth factor (VEGF). (D) Protein levels of VEGF by ELISA in the conditioned medium and the value expressed as pg/ml. $^{*}p \leq 0.05$; $^{**}p \leq 0.01$; $^{***}p \leq 0.001$ when compared to control. $^{\#\#}p \leq 0.01$ when compared to copper 50 µM treatment.

results reveal that similar to copper treatment in ARPE19 cells the choroid RPE tissue response to copper with an increase in SCO1and PGC1β in late cases of AMD. As the number of samples used for mRNA expression was a limiting factor increasing the number will give us a valuable insight.

4. Discussion

Even though, considerable abnormalities are seen in interrelated tissues of photoreceptors, Bruch's membrane and choriocapillaries, major impairment of retinal pigment epithelium (RPE) cellular function leads to AMD pathology [45]. RPE dysfunction has been long credited to oxidative stress and inflammation [46] but recent evidences show that there is regulatory crosstalk between oxidative stress-related transcription factor NRF2 and mitochondria [47]. Our recent study has shown decreased NRF2 expression in the retinal tissue of AMD cases [6]. There are reports on mitochondrial DNA (mtDNA) damage and altered mitochondrial proteins in human donor eyes with AMD [48,49]. Mitochondrial dysfunction seen in donor AMD tissues supports the hypothesis that AMD pathology is driven by defective mitochondria seen in RPE [50]. Mitochondrial damage can release the mitochondrial proteins to the cytoplasm thereby triggering apoptosis and inflammasome activation [51]. Mitochondria have been greatly known for their role in energy production and involvement in the critical cellular homeostasis processes. The homeostatic maintenance of mitochondria requires metal ions like iron and copper [52,53] and imbalance is associated with mitochondrial dysfunction and cardiomyopathy [54,55]. In our study the copper levels were significantly increased in choroid RPE and retina of late AMD cases when compared to its respective controls. The levels of other divalent ions Fe and Zn were decreased. Since copper is important for mitochondrial function, we interrogated the role of copper in AMD pathogenesis using ARPE19 cells as a model.

The influx transporter CTR1 showed a maximal localization in the plasma membrane of ARPE19 cells at 100 µM copper treatment at 24 h and there was an increase in copper uptake. Once copper enters the cell, it binds to metallothioneins and glutathione for storage and to metallochaperones for distributing to specific proteins and intracellular organelles [56]. The mitochondrial chaperones SCO1 which delivers copper to the Cu A and Cu B site of the cytochrome C oxidase in mitochondria [57] showed significant increase at the level of mRNA and protein in our study. But quite interestingly chelating copper did not decrease its expression. But the other mitochondrial chaperone COX11 decreased on chelating copper. SCO1 is a stress response factor [35] and we hypothesis the increase in its expression is mediated by increased ROS generation in both copper and penicillamine treatment. To further understand if CTR1 and SCO1 have some association, both the genes were transiently transfected in RPE cells and treated with copper and we speculate SCO1 to drift away from CTR1 on addition of copper which is another interesting finding which has to be probed further.

Even though the ROS levels were increased with Cu treatment the mitochondrial membrane potential was restored on copper treatment. It is reported that NRF2 plays a crucial role in maintaining cellular redox homeostasis, mitochondrial membrane potential and ATP synthesis and supports the structural and functional integrity of the mitochondria [58]. The transcription factors NRF1&2, PGC1β and TFAM were upregulated and there was a significant increase in cytochrome C oxidase activity in RPE cells treated with copper. NRF1 binds to the specific promoter sites and regulates expression of TFAM [59] the mitochondrial biogenesis regulator [60]. The relative abundance of mitochondria in the copper treated condition was inferred by measuring mtDNA content by COX1/SDHA ratio and the mitochondrial staining.

Copper also triggers PGC1β which is a major regulator of ATP

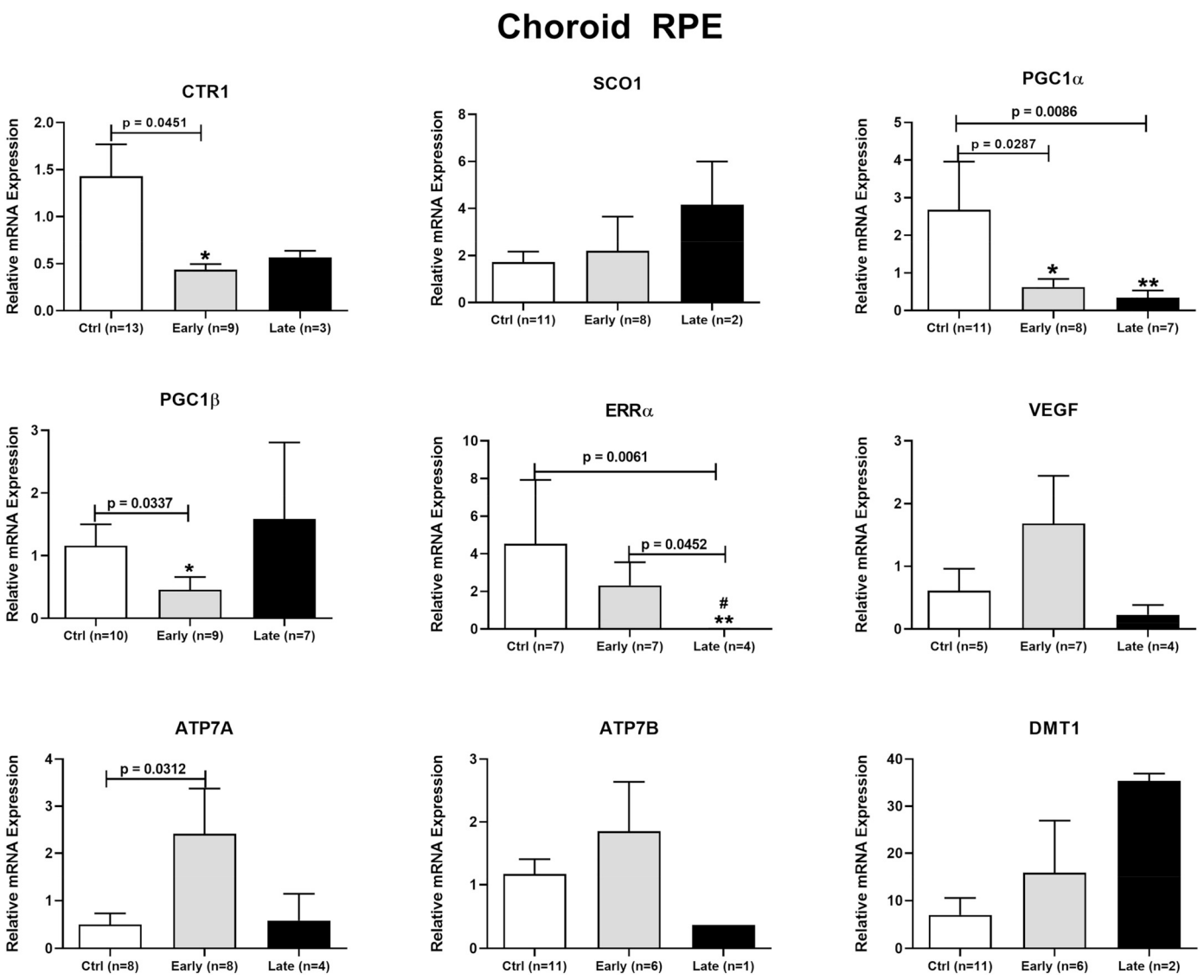

Fig. 8. The mRNA expression levels of copper related factors in the retina and choroid RPE tissues of the ARMD cases. (A) The mRNA expression levels of the copper regulated chaperones and transporters CTR1, ATP7A, ATP7B, SCO1, PGC1α and β, ERRα and VEGF were analyzed in early and late AMD in choroid RPE and (B) Retinal tissues. $*p \leq 0.05$; $**p \leq 0.01$ with Mann Whitney Test.

production in mitochondria [61]. This was supported by increase in the mitochondrial complex 1 copy number on copper treatment. Fibroblasts isolated from patients with complex 1 inhibition showed decreased ATP production with increased oxidative stress and apoptosis [62]. Coussee et al., reported that impairment of complex 1 brings about the decrease of Ca^{2+} uptake and ATP production [63]. PGC1β overexpression leads to a larger induction of MFN2 protein and increased mitochondrial length and mitochondrial fusion rates in wild-type and MFN1 knockout mouse embryonic fibroblasts (MEFs); however, in MFN2 knockout MEFs PGC1β overexpression was unable to increase mitochondrial length demonstrating that MFN2 expression was required to induce these changes in mitochondrial morphology [41]. It is reported that cytochrome C oxidase also increases Mitofusin2 (MFN2) [64]. Mitofusins have been linked to mitochondrial biogenesis and respiratory functions, impacting on cell fate and organism homeostasis [65–67] In our study we observe transcript and protein level increase in MFN2 expression.

But there was a decrease in PGC1α expression with copper treatment. We speculate that the decrease in PCG1α may be due to reduced SIRT1 on copper treatment as reported earlier in human fetal lung fibroblasts and we found that copper chelation augments PGC1α and downregulates PGC1β [68]. SIRT1 is a NAD^+-dependent protein deacetylase, an important regulator in cellular stress response and energy metabolism [69]. PGC1β is positively associated with ERRα and VEGF levels [70]. ERRα has been reported to regulate mitochondrial biogenesis in association with PGC family co-activators via cross-talk with mitogen-activated protein kinase kinases and PI3K/(AKT) signaling [71]. In this study an increase in ERRα was seen along with PGC1β and VEGF which is required for the RPE survival. This is similar to the study which shows PGC1β regulates mitochondrial biogenesis through the NRF1-ERRα axis in C2C12 cells [43].

After getting the telltale from the cell line experiments, the copper transporters and markers of mitochondrial biogenesis were studied in the cadaveric choroid-RPE tissue of the donor AMD cases. We found there was a decrease in CTR1 mRNA expression but the other metal transporter DMT1 expression was significantly increased. SCO1 and PGC1β expression showed increase in late AMD cases. This correlated with the significant increase in copper levels in choroid RPE of late AMD cases.

5. Conclusion

Imbalance in copper homeostasis exert toxicity, oxidative stress, reduced antioxidant mechanism and affect various metabolic functions in circulation and as well as in ocular tissues [72] Evidences show copper depletion might contribute to cellular apoptosis or necrosis as well as mitochondrial dysfunction by impairing the mitochondrial biogenesis [52]. Our study supports this fact that copper does play an important role in mitochondrial biogenesis in RPE cells and we propose that extensive study is required to understand the implication of copper in AMD pathogenesis.

CRediT authorship contribution statement

M. Aloysius Dhivya: Investigation. **S. Aberami:** Investigation. **S. Nikhala Shree:** Investigation. **J. Biswas:** Resources. **Wenjie Liu:** Investigation, Formal analysis. **Joseph Irudayaraj:** Investigation, Formal analysis. **K.N. Sulochana:** Writing - review & editing. **Coral Karunakaran:** Methodology, Formal analysis, Writing - original draft. **S.R. Bharathi Devi:** Methodology, Formal analysis, Writing - original draft.

Declaration of competing interest

The authors declare that they have no known competing financial interests or personal relationships that could have appeared to influence the work reported in this paper.

Acknowledgements

This research was funded by DST sanction number SB/YS/LS-122/2014 and CSIR sanction number 27 (0264/12/EMR-II). Our sincere thanks to Dr. Joseph Irudayaraj Founder Professor of Bioengineering, Department of Bioengineering, UIUC, Urbana-Champaign, IL for his support to perform the SCO1 and CTR1 FLIM FRET analysis in his lab. We thank TRPVB, TANUVAS for helping us with the confocal imaging.

References

[1] R. Narayanan, B.D. Kuppermann, Hot topics in dry AMD, Curr. Pharm. Des. 23 (2017) 542–546, https://doi.org/10.2174/1381612822666161221154424.
[2] G.S. Hageman, K. Gehrs, L.V. Johnson, D. Anderson, Age-related Macular Degeneration (AMD), University of Utah Health Sciences Center, 1995.
[3] Dry vs wet age-related macular degeneration - AMDF, https://www.macular.org/dry-vs-wet-macular-degeneration , Accessed date: 26 February 2020(n.d.).
[4] Y. Chen, M. Bedell, K. Zhang, Age-related macular degeneration, Mol. Interv. 10 (2010) 271–281.
[5] J.M. Flinn, P. Kakalec, R. Tappero, B. Jones, I. Lengyel, Correlations in distribution and concentration of calcium, copper and iron with zinc in isolated extracellular deposits associated with age-related macular degeneration, Metallomics. 6 (2014) 1223–1228, https://doi.org/10.1039/C4MT00058G.
[6] S. Aberami, S. Nikhalashree, M. Bharathselvi, J. Biswas, K.N. Sulochana, K. Coral, Elemental concentrations in Choroid-RPE and retina of human eyes with age-related macular degeneration, Exp. Eye Res. 186 (2019), https://doi.org/10.1016/j.exer.2019.107718.
[7] A. Terman, B. Gustafsson, U.T. Brunk, The lysosomal-mitochondrial axis theory of postmitotic aging and cell death, Chem. Biol. Interact. 163 (2006) 29–37, https://doi.org/10.1016/j.cbi.2006.04.013.
[8] P. Hahn, A.H. Milam, J.L. Dunaief, Maculas affected by age-related macular degeneration contain increased chelatable iron in the retinal pigment epithelium and Bruch's membrane, Arch. Ophthalmol. 121 (2003).
[9] A. Biesemeier, E. Yoeruek, O. Eibl, U. Schraermeyer, Iron accumulation in Bruch's membrane and melanosomes of donor eyes with age-related macular degeneration, Exp. Eye Res. 137 (2015) 39–49, https://doi.org/10.1016/j.exer.2015.05.019.
[10] N.K. Wills, V.M. Sadagopa Ramanujam, N. Kalariya, J.R. Lewis, F.J.G.M. van Kuijk, Copper and zinc distribution in the human retina: relationship to cadmium accumulation, age, and gender, Exp. Eye Res. 87 (2008) 80–88, https://doi.org/10.1016/j.exer.2008.04.013.
[11] M. Ugarte, N.N. Osborne, Zinc in the retina, Prog. Neurobiol. 64 (2001) 219–249, https://doi.org/10.1016/S0301-0082(00)00057-5.
[12] P. Stopa, B. Michalke, A. Chaudhri, U. Reulbach, A.G.M. Ju, F.E. Kruse, E. Zrenner, C. Huchzermeyer, U. Schlo, R. Rejdak, Levels of aqueous humor trace elements in patients with non-exsudative age-related macular degeneration: a case-control study, PLoS One 8 (2013) 1–7, https://doi.org/10.1371/journal.pone.0056734.
[13] J.C. Erie, J.A. Good, J.A. Butz, J.S. Pulido, Reduced zinc and copper in the retinal pigment epithelium and choroid in age-related macular degeneration, Am J Ophthalmol. 147 (2009) 276–282 e1, https://doi.org/10.1016/j.ajo.2008.08.014 (doi:S0002-9394(08)00657-0 [pii]\n).
[14] P. Hahn, Y. Qian, T. Dentchev, L. Chen, J. Beard, Z.L. Harris, J.L. Dunaief, Disruption of ceruloplasmin and hephaestin in mice causes retinal iron overload and retinal degeneration with features of age-related macular degeneration, Proc. Natl. Acad. Sci. U. S. A. 101 (2004) 13850–13855, https://doi.org/10.1073/pnas.0405146101.
[15] R. Gaudana, H.K. Ananthula, A. Parenky, A.K. Mitra, Ocular drug delivery, AAPS J. 12 (2010) 348–360, https://doi.org/10.1208/s12248-010-9183-3.
[16] O. Strauss, The retinal pigment epithelium in visual function, Physiol. Rev. 85 (2005) 845–881, https://doi.org/10.1152/physrev.00021.2004.
[17] M. Subramani, M. Ponnalagu, L. Krishna, N. Jeyabalan, P. Chevour, A. Sharma, C. Jayadev, R. Shetty, N. Begum, G. Archunan, D. Das, Resveratrol reverses the adverse effects of bevacizumab on cultured ARPE-19 cells, Sci. Rep. 7 (2017) 1–16, https://doi.org/10.1038/s41598-017-12496-z.
[18] D. Rajapakse, K. Peterson, S. Mishra, G. Wistow, Serum starvation of ARPE-19 changes the cellular distribution of cholesterol and Fibulin3 in patterns reminiscent of age-related macular degeneration, Exp. Cell Res. 361 (2017) 333–341, https://doi.org/10.1016/j.yexcr.2017.10.036.
[19] D. Han, X. Wu, L. Liu, W. Shu, Z. Huang, Sodium tanshinone IIA sulfonate protects ARPE-19 cells against oxidative stress by inhibiting autophagy and apoptosis, Sci. Rep. 8 (2018) 1–15, https://doi.org/10.1038/s41598-018-33552-2.
[20] H. Liu, W. Liu, X. Zhou, C. Long, X. Kuang, J. Hu, Y. Tang, L. Liu, J. He, Z. Huang, Y. Fan, G. Jin, Q. Zhang, H. Shen, Protective effect of lutein on ARPE-19 cells upon H2O2-induced G2/M arrest, Mol. Med. Rep. 16 (2017) 2069–2074, https://doi.org/10.3892/mmr.2017.6838.
[21] S.C. Leary, D.R. Winge, P.A. Cobine, "Pulling the plug" on cellular copper: the role of mitochondria in copper export, Biochim. Biophys. Acta Mol. Cell Res. 1793 (2009) 146–153, https://doi.org/10.1016/j.bbamcr.2008.05.002.
[23] J. Biswas, R. Raman, Age-related changes in the macula. A histopathological study of fifty Indian donor eyes, Indian J. Ophthalmol. 50 (2002) 201–204 http://www.ncbi.nlm.nih.gov/pubmed/12355694 , Accessed date: 30 September 2019.
[24] The Alabama Age-Related Macular Degeneration Grading System for donor eyes|IOVS|ARVO Journals, https://iovs.arvojournals.org/article.aspx?articleid=2161659 , Accessed date: 26 February 2020(n.d.).
[25] T. Koressaar, M. Remm, Enhancements and modifications of primer design program Primer3, Bioinforma. Appl. Note 23 (2007) 1289–1291, https://doi.org/10.1093/bioinformatics/btm091.
[26] E. de L Rebouças, J.J. do N. Costa, M.J. Passos, J.R. de S. Passos, R. van den Hurk, J.R.V. Silva, Real time PCR and importance of housekeepings genes for normalization and quantification of mRNA expression in different tissues, Brazilian Arch. Biol. Technol. 56 (2013) 143–154, https://doi.org/10.1590/S1516-89132013000100019.
[27] J.P. Rooney, I.T. Ryde, L.H. Sanders, E.H. Howlett, M.D. Colton, K.E. Germ, G.D. Mayer, J.T. Greenamyre, J.N. Meyer, PCR based determination of mitochondrial DNA copy number in multiple species, Methods Mol. Biol. 1241 (2015) 23–38, https://doi.org/10.1007/978-1-4939-1875-1_3.
[28] M. Spinazzi, A. Casarin, V. Pertegato, L. Salviati, C. Angelini, Assessment of mitochondrial respiratory chain enzymatic activities on tissues and cultured cells, Nat. Protoc. 7 (2012) 1235–1246, https://doi.org/10.1038/nprot.2012.058.
[29] A. Eigentler, A. Draxl, A. Wiethüchter, K. Av, B. Lassing, E. Gnaiger, Laboratory protocol: citrate synthase a mitochondrial marker enzyme, www.oroboros.at , Accessed date: 28 February 2020.
[30] W. Liu, E. Biton, A. Pathania, A. Matityahu, J. Irudayaraj, I. Onn, Monomeric cohesin state revealed by live-cell single-molecule spectroscopy, EMBO Rep. 21 (2020), https://doi.org/10.15252/embr.201948211.
[31] W. Liu, Y. Cui, W. Ren, J. Irudayaraj, Epigenetic biomarker screening by FLIM-FRET for combination therapy in ER+ breast cancer, Clin. Epigenetics 11 (2019) 16, https://doi.org/10.1186/s13148-019-0620-6.
[32] B. Haglund, K. Ryckenberg, O. Selinus, G. Dahlquist, Evidence of a relationship between childhood-onset type I diabetes and low groundwater concentration of zinc, Diabetes Care 19 (1996) 873–875, https://doi.org/10.2337/diacare.19.8.873.
[33] N.S. Joo, S.M. Kim, Y.S. Jung, K.M. Kim, Hair iron and other minerals' level in breast cancer patients, Biol. Trace Elem. Res. 129 (2009) 28–35, https://doi.org/10.1007/s12011-008-8281-x.
[34] F. Saleh, A. Behbehani, S. Asfar, I. Khan, G. Ibrahim, Abnormal blood levels of trace elements and metals, DNA damage, and breast cancer in the state of Kuwait, Biol. Trace Elem. Res. 141 (2011) 96–109, https://doi.org/10.1007/s12011-010-8724-z.
[35] A. Ekim Kocabey, L. Kost, M. Gehlhar, G. Rödel, U. Gey, Mitochondrial Sco proteins are involved in oxidative stress defense, Redox Biol. 21 (2019), https://doi.org/10.1016/j.redox.2018.101079.
[36] C.J. Hlynialuk, B. Ling, Z.N. Baker, P.A. Cobine, L.D. Yu, A. Boulet, T. Wai, A. Hossain, A.M. ElZawily, P.J. McFie, S.J. Stone, F. Diaz, C.T. Moraes, D. Viswanathan, M.J. Petris, S.C. Leary, The mitochondrial metallochaperone SCO1 is required to sustain expression of the high-affinity copper transporter CTR1 and preserve copper homeostasis, Cell Rep. 10 (2015) 933–943, https://doi.org/10.1016/j.celrep.2015.01.019.
[37] Q. Ma, Role of Nrf2 in oxidative stress and toxicity, Annu. Rev. Pharmacol. Toxicol. 53 (2013) 401–426, https://doi.org/10.1146/annurev-pharmtox-011112-140320.
[38] N. Robledinos-Antón, R. Fernández-Ginés, G. Manda, A. Cuadrado, Review Article Activators and Inhibitors of NRF2: A Review of Their Potential for Clinical Development, (2019), https://doi.org/10.1155/2019/9372182.
[39] M.O. Song, M.D. Mattie, C.H. Lee, J.H. Freedman, The role of Nrf1 and Nrf2 in the

regulation of copper-responsive transcription, Exp. Cell Res. 322 (2014) 39–50, https://doi.org/10.1016/j.yexcr.2014.01.013.
[40] N. Gleyzer, K. Vercauteren, R.C. Scarpulla, Control of mitochondrial transcription specificity factors (TFB1M and TFB2M) by nuclear respiratory factors (NRF-1 and NRF-2) and PGC-1 family coactivators, Mol. Cell. Biol. 25 (2005) 1354–1366, https://doi.org/10.1128/MCB.25.4.1354-1366.2005.
[41] M. Liesa, B. Bord-d'Água, G. Medina-Gómez, C.J. Lelliott, J.C. Paz, M. Rojo, M. Palacín, A. Vidal-Puig, A. Zorzano, Mitochondrial fusion is increased by the nuclear coactivator PGC-1β, PLoS One 3 (2008), https://doi.org/10.1371/journal.pone.0003613.
[42] J. Igarashi, R. Okamoto, T. Yamashita, T. Hashimoto, S. Karita, K. Nakai, Y. Kubota, M. Takata, F. Yamaguchi, M. Tokuda, N. Sakakibara, I. Tsukamoto, R. Konishi, K. Hirano, A key role of PGC-1 α transcriptional coactivator in production of VEGF by a novel angiogenic agent COA-Cl in cultured human fibroblasts, Physiol. Rep. 4 (2016) e12742, https://doi.org/10.14814/phy2.12742.
[43] D. Shao, Y. Liu, X. Liu, L. Zhu, Y. Cui, A. Cui, A. Qiao, X. Kong, Y. Liu, Q. Chen, N. Gupta, F. Fang, Y. Chang, PGC-1 beta-regulated mitochondrial biogenesis and function in myotubes is mediated by NRF-1 and ERR alpha, Mitochondrion. 10 (2010) 516–527, https://doi.org/10.1016/j.mito.2010.05.012.
[44] L. Chitra, R. Boopathy, Altered mitochondrial biogenesis and its fusion gene expression is involved in the high-altitude adaptation of rat lung, Respir. Physiol. Neurobiol. 192 (2014) 74–84, https://doi.org/10.1016/j.resp.2013.12.007.
[45] J.Z. Nowak, Age-related macular degeneration (AMD): pathogenesis and therapy., Pharmacol. Rep. 58 353–63. http://www.ncbi.nlm.nih.gov/pubmed/16845209 (accessed August 21, 2019) (n.d.).
[46] S. Datta, M. Cano, K. Ebrahimi, L. Wang, J.T. Handa, The impact of oxidative stress and inflammation on RPE degeneration in non-neovascular AMD, Prog. Retin. Eye Res. 60 (2017) 201–218, https://doi.org/10.1016/j.preteyeres.2017.03.002.
[47] I. Geun Ryoo, M.K. Kwak, Regulatory crosstalk between the oxidative stress-related transcription factor Nfe2l2/Nrf2 and mitochondria, Toxicol. Appl. Pharmacol. 359 (2018) 24–33, https://doi.org/10.1016/j.taap.2018.09.014.
[48] P.P. Karunadharma, C.L. Nordgaard, T.W. Olsen, D.A. Ferrington, Biochemistry and molecular biology mitochondrial DNA damage as a potential mechanism for age-related macular degeneration, Invest. Ophthalmol. Vis. Sci. 51 (2010) 5470–5479, https://doi.org/10.1167/iovs.10-5429.
[49] C.L. Nordgaard, K.M. Berg, R.J. Kapphahn, C. Reilly, X. Feng, T.W. Olsen, D.A. Ferrington, Proteomics of the retinal pigment epithelium reveals altered protein expression at progressive stages of age-related macular degeneration, Investig. Ophthalmol. Vis. Sci. 47 (2006) 815–822, https://doi.org/10.1167/iovs.05-0976.
[50] J. Feher, I. Kovacs, M. Artico, C. Cavallotti, A. Papale, C. Balacco, Mitochondrial alterations of retinal pigment epithelium in age-related macular degeneration, Neurobiol. Aging 27 (2006) 983–993, https://doi.org/10.1016/j.neurobiolaging.2005.05.012.
[51] K. Shimada, T.R. Crother, J. Karlin, J. Dagvadorj, N. Chiba, S. Chen, V.K. Ramanujan, A.J. Wolf, L. Vergnes, D.M. Ojcius, A. Rentsendorj, M. Vargas, C. Guerrero, Y. Wang, K.A. Fitzgerald, D.M. Underhill, T. Town, M. Arditi, Oxidized mitochondrial DNA activates the NLRP3 inflammasome during apoptosis, Immunity. 36 (2012) 401–414, https://doi.org/10.1016/j.immuni.2012.01.009.
[52] W. Xu, T. Barrientos, N.C. Andrews, Iron and copper in mitochondrial diseases, Cell Metab. 17 (2013) 319–328, https://doi.org/10.1016/j.cmet.2013.02.004.
[53] Z.N. Baker, P.A. Cobine, S.C. Leary, The mitochondrion: a central architect of copper homeostasis, Metallomics. 9 (2017) 1501–1512, https://doi.org/10.1039/c7mt00221a.
[54] B.E. Kim, M.L. Turski, Y. Nose, M. Casad, H.A. Rockman, D.J. Thiele, Cardiac copper deficiency activates a systemic signaling mechanism that communicates with the copper acquisition and storage organs, Cell Metab. 11 (2010) 353–363, https://doi.org/10.1016/j.cmet.2010.04.003.
[55] N. Hegde, M.W. Rich, C. Gayomali, The cardiomyopathy of iron deficiency, Texas Hear. Inst. J. 33 (2006) 340–344 http://www.ncbi.nlm.nih.gov/pubmed/17041692, Accessed date: 21 August 2019.
[56] H.Ö., D.J. Thiele, How copper traverses cellular membranes through the mammalian copper transporter 1, Ctr1, (2015), pp. 32–41, https://doi.org/10.1111/nyas.12371.How.
[57] A. Timón-Gómez, E. Nývltová, L.A. Abriata, A.J. Vila, J. Hosler, A. Barrientos, Mitochondrial cytochrome c oxidase biogenesis: recent developments, Semin. Cell Dev. Biol. 76 (2018) 163–178, https://doi.org/10.1016/j.semcdb.2017.08.055.
[58] A.T. Dinkova-Kostova, A.Y. Abramov, The emerging role of Nrf2 in mitochondrial function, Free Radic. Biol. Med. 88 (2015) 179–188, https://doi.org/10.1016/j.freeradbiomed.2015.04.036.
[59] J.V. Virbasius, R.C. Scarpulla, Activation of the human mitochondrial transcription factor A gene by nuclear respiratory factors: a potential regulatory link between nuclear and mitochondrial gene expression in organelle biogenesis, Proc. Natl. Acad. Sci. U. S. A. 91 (1994) 1309–1313, https://doi.org/10.1073/pnas.91.4.1309.
[60] I. Irrcher, P.J. Adhihetty, A.M. Joseph, V. Ljubicic, D.A. Hood, Regulation of mitochondrial biogenesis in muscle by endurance exercise, Sport. Med. 33 (2003) 783–793, https://doi.org/10.2165/00007256-200333110-00001.
[61] T. Gali Ramamoorthy, G. Laverny, A.-I. Schlagowski, J. Zoll, N. Messaddeq, J.-M. Bornert, S. Panza, A. Ferry, B. Geny, D. Metzger, The transcriptional coregulator PGC-1β controls mitochondrial function and anti-oxidant defence in skeletal muscles, Nat. Commun. 6 (2015) 10210, https://doi.org/10.1038/ncomms10210.
[62] A. Saada, M. Bar-Meir, C. Belaiche, C. Miller, O. Elpeleg, Evaluation of enzymatic assays and compounds affecting ATP production in mitochondrial respiratory chain complex I deficiency, Anal. Biochem. 335 (2004) 66–72, https://doi.org/10.1016/j.ab.2004.08.015.
[63] E. Coussee, P. De Smet, E. Bogaert, I. Elens, P. Van Damme, P. Willems, W. Koopman, L. Van Den Bosch, G. Callewaert, G37R SOD1 mutant alters mitochondrial complex I activity, Ca2+ uptake and ATP production, Cell Calcium 49 (2011) 217–225, https://doi.org/10.1016/j.ceca.2011.02.004.
[64] W. Yin, R. Li, X. Feng, Y. James Kang, The involvement of cytochrome c oxidase in mitochondrial fusion in primary cultures of neonatal rat cardiomyocytes, Cardiovasc. Toxicol. (2018), https://doi.org/10.1007/s12012-018-9447-1.
[65] E. Schrepfer, L. Scorrano, Mitofusins, from mitochondria to metabolism, Mol. Cell 61 (2016) 683–694, https://doi.org/10.1016/j.molcel.2016.02.022.
[66] M. Liesa, O.S. Shirihai, Mitochondrial dynamics in the regulation of nutrient utilization and energy expenditure, Cell Metab. 17 (2013) 491–506, https://doi.org/10.1016/j.cmet.2013.03.002.
[67] S. Pich, D. Bach, P. Briones, M. Liesa, M. Camps, X. Testar, M. Palacín, A. Zorzano, The Charcot-Marie-Tooth type 2A gene product, Mfn2, up-regulates fuel oxidation through expression of OXPHOS system (n.d.). doi:https://doi.org/10.1093/hmg/ddi149.
[68] L. Matos, A.M. Gouveia, H. Almeida, Resveratrol attenuates copper-induced senescence by improving cellular proteostasis, Oxidative Med. Cell. Longev. 2017 (2017) 1–12, https://doi.org/10.1155/2017/3793817.
[69] X. Guo, M. Kesimer, G. Tolun, X. Zheng, Q. Xu, J. Lu, J.K. Sheehan, J.D. Griffith, X. Li, The NAD+-dependent protein deacetylase activity of SIRT1 is regulated by its oligomeric status, Sci. Rep. 2 (2012), https://doi.org/10.1038/srep00640.
[70] G.C. Rowe, C. Jang, I.S. Patten, Z. Arany, Pgc-1β regulates angiogenesis in skeletal muscle, Am. J. Physiol. - Endocrinol. Metab. 301 (2011), https://doi.org/10.1152/ajpendo.00681.2010.
[71] H.S. Ranhotra, Estrogen-related receptor alpha and mitochondria: tale of the titans, J. Recept. Signal Transduct. 35 (2015) 386–390, https://doi.org/10.3109/10799893.2014.959592.
[72] S. Potocki, M. Rowinska-Zyrek, D. Witkowska, M. Pyrkosz, A. Szebesczyk, K. Krzywoszynska, H. Kozlowski, Metal transport and homeostasis within the human body: toxicity associated with transport abnormalities, Curr. Med. Chem. 19 (2012) 2738–2759, https://doi.org/10.2174/092986712800609698.